19th Australasian Fluid Mechanics Conference
Melbourne, Australia
8-11 December 2014

Dynamic Mode Decomposition of Near Nozzle Instabilities in Large-Eddy Simulations of Under-Expanded Circular Jets.

P. C. Stegeman[1], J. Soria[1] and A. Ooi[2]

[1]Laboratory for Turbulence Research in Aerospace and Combustion, Department of Mechanical and Aerospace Engineering,
Monash University, VIC 3800, AUSTRALIA

[2]Department of Mechanical Engineering,
University of Melbourne, Parkville, VIC 3052, AUSTRALIA

Abstract

This paper undertakes a dynamic mode decomposition of under-expanded jets in order to extract fundamental instability modes near the nozzle from the flow field. Topological information and evolution of the extracted modes are then determined as a function of axial distance from the nozzle. This information will allow for the extension of models used to predict the acoustic radiation processes of such jets.

Introduction

Acoustic feedback in under-expanded free-jets has been a topic of research over the last five decades with a global summary provided in [9]. It is understood that the feedback loop is due to large scale coherent structures present in the shear layer interacting with the core shock cells and that the attenuation of these structures may significantly reduce the broadband and discreet (Screech) noise generated. However the details of the dynamics of these large scale structures and the significant changes that occur due to a change in the jets nozzle pressure ratio (NPR) are still not well understood. In order to gain a better understanding of the topology and dynamics of these structures the dynamic mode decomposition (DMD) technique will be applied to high resolution numerical datasets.

Reduced models are often used to determine the generation of acoustic waves due to the shock-vortex interaction [8] as well as due to Mach wave radiation [10]. Such models assume an uniform, isotropic and regular vortex structure in the shear layer. However in reality, coherent structures do not fit into these categories. Therefore this paper seeks to determine the topology of the coherent structures in such a jet for the future extension of the models mentioned.

In this study we consider a purely convergent under-expanded circular free jet with nozzle pressure ratios NPR=$\{2.2, 3.4\}$ and a nozzle lip thickness $t_n/d = 1/3$ where $d = 15$mm is the nozzle diameter.

Numerical Dataset

The free-jet dataset used in this study is the result of a three dimensional hybrid large-eddy simulation on a non-uniform structured cylindrical grid. For spatial differentiation the hybrid solver employs a sixth order central finite difference scheme for smooth regions and a fifth order weighted essentially non-oscillatory scheme with local Lax-Friedrichs flux splitting in discontinuous regions. Temporal integration is performed using a fourth order five step Runge-Kutta scheme. The sub-grid scale terms where computed using Germanos dynamic model with the adjustments made by Lilly [3]. The domain consists of approximately 16.4 million nodes with the spatial extent of $30d$ downstream and $15d$ the radial direction. Locally one-dimensional inviscid compressible boundary conditions defined in [6] are used for the adiabatic nozzle wall and outflow regions. Sponge regions are employed near the outflow boundary were the flow field is forced to a self-similar incompressible jet solution that has been determined a priori. The jet inlet velocity profile was modeled using the hyperbolic-tangent function found in [1] while the temperature profile was determined using the Crocco-Busemann relationship [7]. No inlet turbulence has been applied. The $NPR = 2.2$ and $NPR = 3.4$ cases have completed approximately 48,500 and 61,950 time steps or $t/t_0 = 48$ and $t/t_0 = 31$ turn-over times respectively where $t_0 = d/u_j$ and u_j is the nozzle exit velocity ($\approx 310m/s$).

Mean and Temporal Statistics

Mean velocity and fluctuating velocity profiles are provided in figure 1 where it may be seen that the first shock reflecting points are $0.62d$ and $1.41d$ for the $NPR = 2.2$ and $NPR = 3.4$ respectively. Spectra of the fluctuating velocity for $NPR = 2.2$ and $NPR = 3.4$ that was sampled at the center of the shear layer at positions $x = 0.9d$ and $x = 1.9d$ respectively, may be seen in figure 2. For $NPR = 2.2$ the first instability mode is visible at $St = 1.79$ with its first harmonic at $St = 3.63$. The peak for the first instability mode in the $NPR = 3.4$ case is not as pronouced but may be seen at $St \approx 1.46$ with its first harmonic at 2.98. These results compare well with linear stability theory examined by Michalke [4], however for Screeching jets the Strouhal number expected is approximately $St \approx 0.4$ [5]. It has been reasoned that this is due to the lack of a nozzle lip at the outflow boundary region which is preventing or substantially modifying the receptivity of the shear layer to the acoustic waves generated by the vortex shock interaction. Therefore in this paper the instability modes investigated are those inherent to the jet rather than the modes expected to be generated by the screech feedback mechanism. Modified boundary conditions are currently being investigated to achieve the screeching modes.

Dynamic Mode Decomposition

Dynamic mode decomposition (DMD) calculates the Koopman modes describing the transient linear components of a non-linear flow field. We may decompose a transient non-linear flow field as

$$\frac{\partial \mathbf{u}'}{\partial t}(\mathbf{x},t) = \mathbf{M}\mathbf{u}'(\mathbf{x},t) + \mathbf{f}(\mathbf{x},t) \tag{1}$$

where $\mathbf{M}$ is a linear operator and $\mathbf{f}$ contains the non-linear residuals not captured by $\mathbf{M}$. It is then assumed that the flow field may be represented by a set of harmonic oscillators, individually represented as

$$\mathbf{u}'(\mathbf{x},t) = \hat{\mathbf{u}}(\mathbf{x}) K e^{-i\Omega t} \tag{2}$$

The two equations above lead to an eigenvalue problem which produces a set of spatial eigenvectors ($\hat{\mathbf{u}}$) with corresponding eigenvalues (Ω) describing the temporal frequencies and

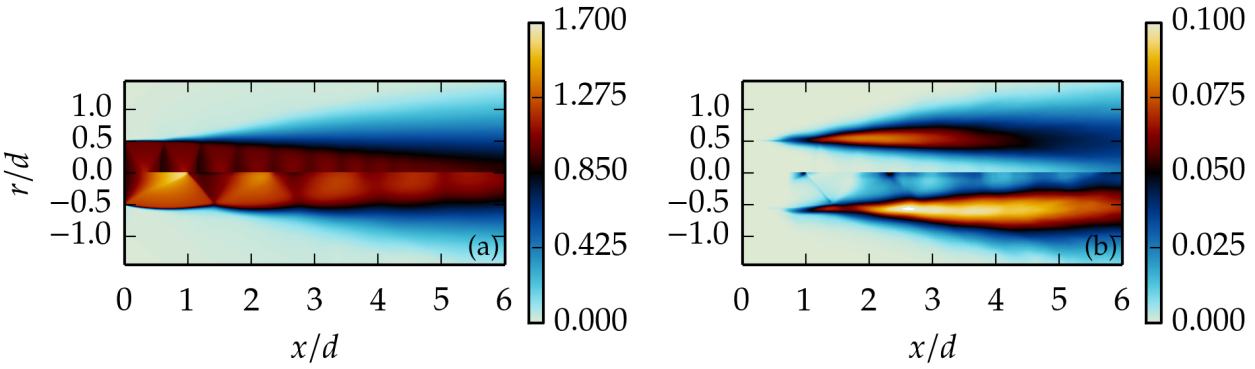

Figure 1. Temporal mean of the velocity (a) and fluctuting velocity (b) for $NPR = 2.2$ (top half) and $NPR = 3.4$ (bottom half).

growth/decay rates associated with each mode. It is expected that the screech instabilities will not exhibit any globally unstable growth or decay as they are a part of a limit cycle and therefore the DMD eigenvalues representing these modes will lie on the unit circle of the complex plane. The method of projecting DMD modes onto a proper orthogonal decomposition mode basis as outlined in [2] is utilized in order to reduce the computational effort of the analysis.

DMD modes were extracted for each case at the positive and negative peak frequencies found in the spectral analysis (See figure 2). The temporal evolution of each mode was generated by reconstructing them at different phases (ϕ) over their cycle. Iso-surfaces and a half plane contour map of planar vorticity (ω_θ) for $NPR = 2.2$ may be seen in figure 3. Near the nozzle it can be clearly seen that the mode is toroidal with only slight variations in the azimuthal direction. $NPR = 3.4$ exhibits a similar toroidal mode. Both cases exhibit vortex pairs close to the nozzle which merge at axial positions of $x \approx 0.8d$ and $x \approx 1.4$ respectively.

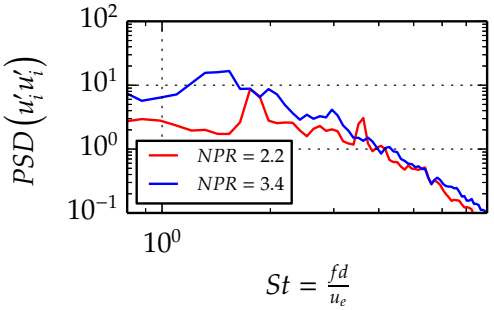

Figure 2. Flutuating velocity spectra for both cases sampled at the center of the shear layer in the center of the second shock cell.

Characterisation of Near-Nozzle Coherent Structures

In order to characterise the topology of the vortical structures an algorithm was created to determine the location of the peak planar vorticity for each coherent structure in each azimuthal plane of the generated DMD modes. A brief overview of the steps the algorithm takes in identifying these shapes follows:

- The maximum planar vorticity is found along each axial plane and the samples below 40% of that maximum are discarded.
- A coherent structure map is generated using a clustering algorithm and discarding structures that do not span the entire azimuthal direction.
- For each coherent structure the local position of maximum vorticity is found (x_c, r_c).
- For a range of angles within $[0, \pi)$ from the jet axis, rays are projected forward and backward to determine the structure's diameter (d_c) at that angle.

An example of the identified features in a single plane can be seen in figure 4. White circles represent the position of the local maximum for a given vortex structure and the dashed lines are representative of the structures size. Due to the weak nature of the vorticies close to the nozzle outlet the identification algorithm becomes less accurate. As will be seen this leads to some spurious noise in the extracted data in these regions.

The variaton of the coherent structures' axial and radial position in the azimuthal direction is plotted in figure 5 as a function of the mean axial position. In both cases the variation is low closer to the nozzle representing fewer azimuthal variations in the toroidal structure. At the shock reflection point in both cases the radial variation increases significantly and recovers within $0.2 - 0.5d$. Increasing variations along the axial direction is likely to be representative of the breakdown of the vortical structure.

As the azimuthal variation of the structures are small in our sampled region the evolution of the structures' shape and intensity properties are determined using their mean in the azimuthal direction. Figures 6, 7 and 8 are plots of the minimum/maximum structure diameters, structure orientation and peak vorticity relative to the maximum as functions of the mean axial position of each structure. As may be seen in figure 6, the anisotropy of the vortex (ratio of minimum to maximum diameters) decreases significantly at the shock reflection point. For both cases the vortex pairs seem to wrap around each other and merge just downstream of the shock reflection point. This may be due to the modulation of the inner vortex at the shock reflection point which rapidly breaks the pair's symmetry. This effect may also be more clearly seen in figure 7 where the orientation of the vortex flips just downstream of the shock reflection point. In both cases there are two distinct linear growth regions of peak vorticity before the first shock reflection point. The maximum peak vorticity occurs at the shock reflection point after which the vorticies loose strength. For the vortex pairs the outer vortex has a lower peak vorticity than the inner vortex, this signifies that there is more energy being transferred to the inner vortex,

possibly due to the varying mean velocity gradients in the jet core.

From this data we can see that the shock reflection point has a pronounced effect on the vortex topology and intensity. Prior acoustic modeling of such jets do not fully account for this modulationt which may have large effects on their predictive power. Further work will be completed to reduce the near nozzle scattering due to improper identification of the vorticies' topologies in this region.

Conclusions

In this paper we have classified the evolution of the topology of coherent structures near the nozzle of two under-expanded free jets using temporal modes captured by dynamic mode decomposition. The data generated in this analysis will allow for the extension of current acoustic models of such jets by increasing the complexity of the modeled coherent structures.

Acknowledgements

This research was supported under Australian Research Council's Discovery Projects funding scheme (project number DP1096474) and was undertaken with the assistance of resources provided at the NCI National Facility systems at the Australian National University through the National Computational Merit Allocation Scheme supported by the Australian Government.

References

[1] Bodony, D. and Lele, S., On using large-eddy simulation for the prediction of noise from cold and heated turbulent jets., *Phys. Fluids*, **17**, 2005, 85–103.

[2] Kitsios, V., Buchmann, N. A., Atkinson, C. A., Frederiksen, J. S. and Soria, J., Recovery of the koopman modes of a leading-edge separated airfoil flow via a proper orthogonal decomposition rank reduction., in *Instability and Control of Massively Separated Flows*, Prato, Italy, 2013.

[3] Lilly, D., A proposed modification of the germano subgrid-scale closure method., *Physics of Fluids*, **4**, 1992, 633.

[4] Michalke, A., Survey on jet instability theor, *Prog. Aerospace Sci.*, **21**, 1984, 159–199.

[5] Mitchell, D., *Coherent structure and shock vortex interaction in the screeching supersonic jet.*, Ph.D. thesis, Department of Mechanical and Aerospace Engineering, Monash University, 2013.

[6] Poinsot, T., Boundary conditions for direct simulations of compressible viscous flows, *J. Comput. Phys.*, **99**, 1992, 352.

[7] Schlichting, H. and Gersten, K., *Boundary Layer Theory*, Springer, 2000.

[8] Suzuki, T. and Lele, S. K., Shock leakage through an unsteady vortex-laden mixing layer: Application to jet screech, in *7th AIAA/CEAS Aeroacoustics Conference*, 2001.

[9] Tam, C. K. W., Supersonic jet noise, *Annu Rev Fluid Mech*, **27**, 1995, 17–43.

[10] Tam, C. K. W., Parrish, S. A. and Viswanathan, K., The harmonics of jet screech tones, in *19th AIAA/CEAS Aeroacoustics Conference*, 2013.

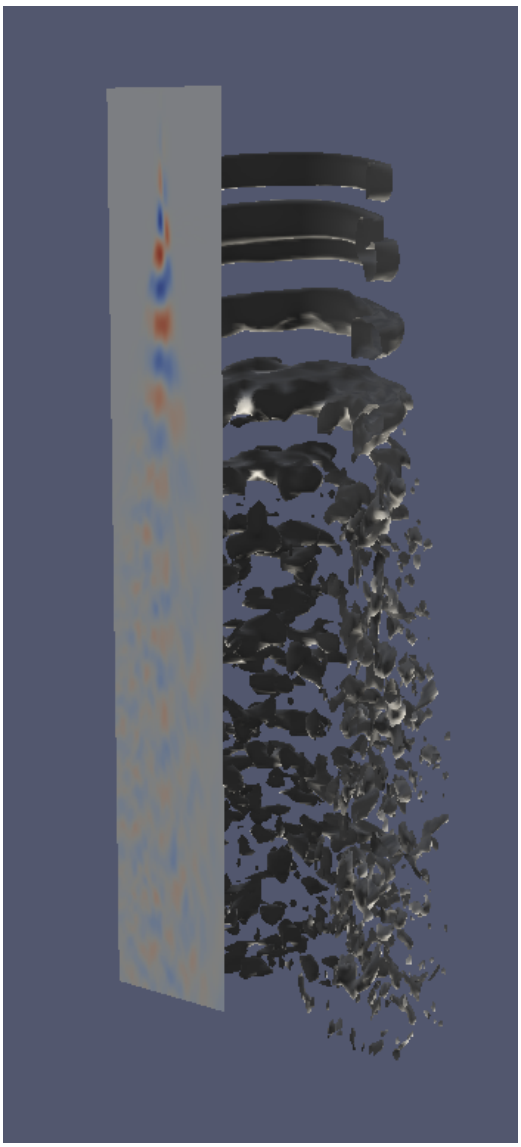

Figure 3. Iso-surfaces and Iso-contours of planar vorticity in DMD mode for $NPR = 2.2$. Iso-surface level is approximately $1/10$ of the maximum.

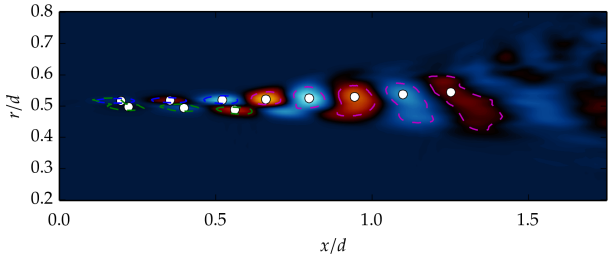

Figure 4. Contour image of planar vorticity in DMD mode for $NPR = 2.2$ and a phase of $\phi = 0$. White circles represent the position of the local maximum for a given vortex structure and the dashed lines represent the representative size of the structures where the planar vorticity has dropped to half its maximum.

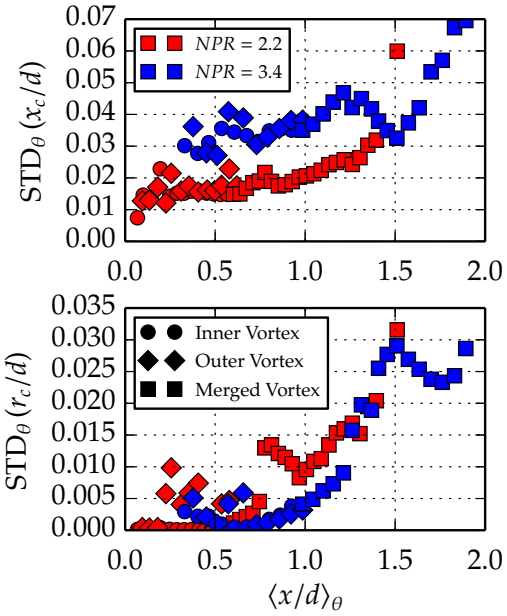

Figure 5. Standard deviation of the azimuthal mean axial (top) and radial (bottom) position of the vortex structures.

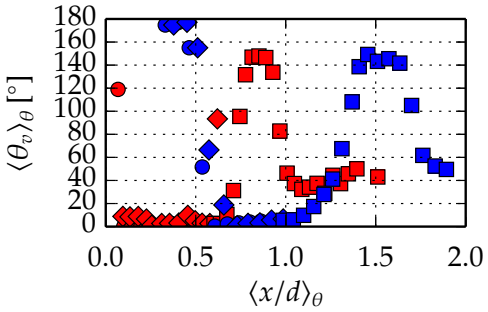

Figure 7. Azimuthal mean rotation of the maximum diameter axis of the vortex structures.

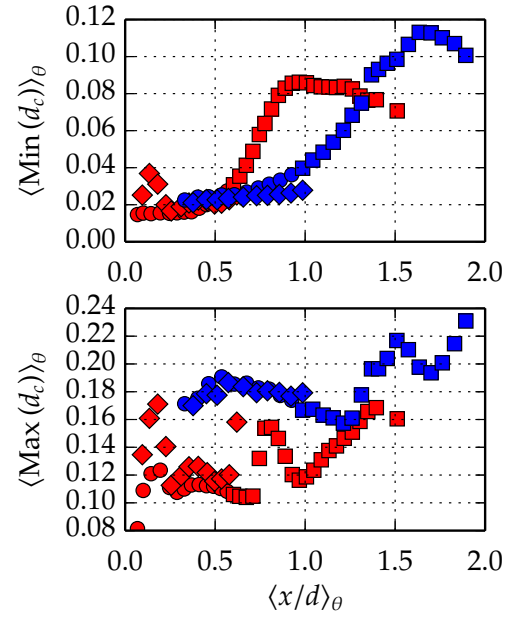

Figure 6. Azimuthal mean minimum (top) and maximum (bottom) diameters of the vortex structures.

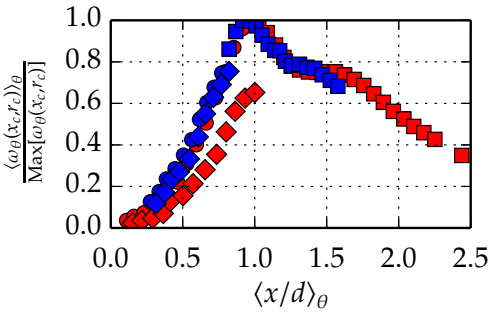

Figure 8. Azimuthal mean of the peak planar voriticty of the vortex structures relative to the maximum in each case.